

Plasma–Particle Interactions in a Laser-Induced Plasma: Implications for Laser-Induced Breakdown Spectroscopy

V. Hohreiter and D. W. Hahn*

Department of Mechanical and Aerospace Engineering, University of Florida, Gainesville, Florida 32611-6300

The interaction between laser-induced plasmas and individual particles controls the rate of particle dissociation and subsequent atomic diffusion and emission processes, with implications for single-particle spectroscopy, as well as materials synthesis and other plasma sources. It is demonstrated through quantitative plasma imaging studies that discrete particles dissociate on a time scale of tens of microseconds within plasmas formed by 300-mJ Nd:YAG laser pulses. Significant spatial nonhomogeneity, as measured by localized atomic emission from particle-derived calcium atoms, persists on a comparable time scale, providing a measure of their average atomic diffusion rate of 0.04 m²/s. In addition, the resulting calcium atomic emission is explored using image analysis as well as traditional spectroscopic analysis.

Laser-induced breakdown spectroscopy (LIBS), or laser-induced plasma spectroscopy, is applicable to the elemental analysis of solid and gaseous samples, including aerosol-laden systems. Historically, LIBS has been implemented using the ensemble-averaged spectra resulting from many hundreds to thousands of laser pulses, as reported in a number of research and review papers.^{1–5} Such an approach greatly improves the signal-to-noise ratio for relatively homogeneous systems; however, aerosol analysis under dilute particle loadings can present unique problems to this LIBS methodology. In response, more recent studies have reported LIBS for aerosol analysis using single-shot conditional spectral processing schemes to effectively sample aerosol populations, thereby yielding discrete particle analysis.^{6–7} Successful implementation of single-shot, LIBS-based aerosol sensing has been reported in several studies of ambient air particulate matter, where particles containing aluminum, calcium, chromium, magnesium, and sodium were detected at analyte masses in the low-femtogram range,^{8–9} as well as more recent measurements of bioaerosols.^{10–11}

The further evolution of laser-induced plasma spectroscopy as an effective technique for the analysis of aerosol systems is dependent on the ability to accurately quantify the presence and concentration of analyte species within individual and small groups of particles. The primary factors challenging LIBS-based aerosol analysis include the fact that small aerosol particles (~100 nm to ~1 μm) may contain only a few femtograms of analyte and that laser-induced plasmas are known to experience large shot-to-shot fluctuations in combination with significant spectral noise, thereby reducing the associated method detection limit. A fundamental step in advancing the LIBS technique is that more be known about the physics of the plasma–particle interactions on a single-plasma, single-particle basis.

Of particular interest are the physical processes and time scales of particle dissociation within a laser-induced plasma and subsequent spatial diffusion of analyte species throughout the plasma. Throughout this report, we use the term particle dissociation as a general description that may encompass a variety of complex processes including particle melting and vaporization, fragmentation, sublimation, molecular ionization and dissociation, and atomic ionization, as well as concomitant heat and mass transfer. As reported in recent modeling efforts, species dissociation and analyte spectral emission within a laser-induced plasma are commonly assumed to occur in a temporally instantaneous and spatially homogeneous way,^{12–14} which significantly reduces the mathematical complexity of such models. In a recent study, however, it was demonstrated that a magnesium-containing aerosol revealed spatially nonhomogeneous atomic emission, as based on spectroscopic analysis of plasma emission collected by an ordered fiber-optic array.¹⁵ In another study, it was shown that micrometer-sized silica particles revealed a clear departure from a linear analyte mass response within a laser-induced plasma for particles greater than ~2 μm.¹⁶ The current study, using a combination of plasma imaging and spectroscopy, addresses the issue of spatially nonhomogeneous atomic emission originating

* To whom correspondence should be addressed: E-mail: dwhahn@ufl.edu.

- (1) Radziemski, L. J.; Loree, T. R.; Cremers, D. A.; Hoffman, N. M. *Anal. Chem.* **1983**, *55*, 1246.
- (2) Neuhauser, R. E.; et al. *Anal. Chim. Acta* **1997**, *346*, 37.
- (3) Sneddon, J.; Lee, Y.-I. *Anal. Lett.* **1999**, *32*, 2143.
- (4) Rusak, D. A.; Castle, B. C.; Smith, B. W.; Winefordner, J. D. *Crit. Rev. Anal. Chem.* **1997**, *27*, 257.
- (5) Lee, W. B.; Wu, J. Y.; Sneddon, J. *Appl. Spectrosc. Rev.* **2004**, *39*, 27.
- (6) Hahn, D. W. *Appl. Phys. Lett.* **1998**, *72*, 2960.
- (7) Hahn, D. W.; Lunden, M. M. *Aerosol Sci. Technol.* **2000**, *33*, 30.
- (8) Carranza, J. E.; Fisher, B. T.; Yoder, G. D.; Hahn, D. W. *Spectrochim. Acta, Part B* **2001**, *56*, 851.

- (9) Lithgow, G. A.; Robinson, A. L.; Buckley, S. G. *Atmos. Environ.* **2004**, *38*, 3319.
- (10) Hybl, J. D.; Lithgow, G. A.; Buckley, S. G. *Appl. Spectrosc.* **2003**, *57*, 1207.
- (11) Dixon, P. B.; Hahn, D. W. *Anal. Chem.* **2004**, *77*, 631.
- (12) Ho, J. R.; Grigoropoulos, C. P.; Humphrey, J. A. C. *J. Appl. Phys.* **1996**, *79*, 7205.
- (13) Itina, T. E.; Hermann, J.; Delaporte, Ph.; Sentis, M. *Appl. Surf. Sci.* **2003**, *208*, 27.
- (14) Gornushkin, I. B.; et al. *Spectrochim. Acta, Part B* **2004**, *59*, 401.
- (15) Lithgow, G. A.; Buckley, S. G. *Appl. Phys. Lett.* **2005**, *87*, 1.
- (16) Carranza, J. E.; Hahn, D. W. *Anal. Chem.* **2002**, *74*, 5450.

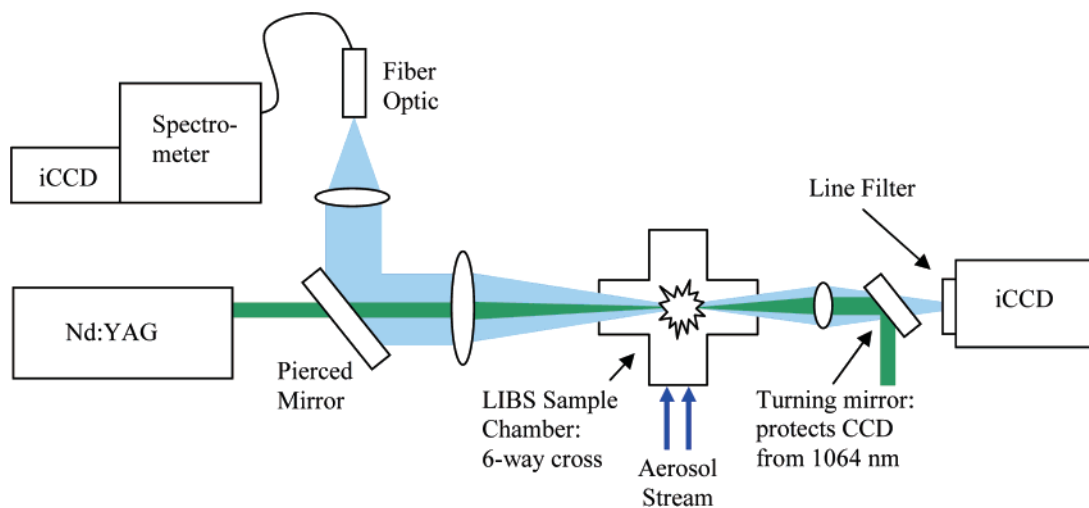


Figure 1. Experimental configuration.

from an aerosol particle within a laser-induced plasma and quantifies a diffusion time scale for both physical aerosol particle dissociation and the ensuing aerosol-derived atomic emission.

EXPERIMENTAL METHODS

For all experiments, a 1064-nm Q-switched Nd:YAG laser with a 10-ns pulse width and 300 mJ/pulse was focused using a 50-mm-diameter, 75-mm-focal length, UV-grade fused-silica lens to create the laser-induced plasma inside a sealed, stainless steel six-way vacuum cross (Huntington Labs), which functioned as the LIBS sample chamber. A nebulized solution of borosilicate glass microspheres (Duke Scientific, No. 9002) in ultrapure deionized water was fed into the chamber using dry, HEPA-filtered air as the carrier gas stream. The nebulized solution and carrier gas stream were mixed inside a 0.8-m-long drying tube to ensure complete desolvation of the nebulized liquid droplets prior to entry into the LIBS sample chamber, thereby producing a dry stream of aerosolized microspheres. The diameter of the borosilicate microspheres was specified by the manufacturer as $2.0 \pm 0.7 \mu\text{m}$, with glass density of 2.50 g/cm^3 , and a dry bulk powder number density of 9.5×10^{10} particles/g. The sphericity and size distribution was confirmed via high-resolution optical microscopy, although no quantitative analysis was recorded. Calcium, a minor constituent of borosilicate glass present as residual lime (CaO), was the analyte of interest for all experiments. Typical lime concentrations for borosilicate glass (in which boric oxide, B_2O_3 , generally replaces the soda in soda-lime glass) are reported in the range from ~ 0.1 to $\sim 1\%$ by mass.

A schematic of the experimental system is shown in Figure 1. Plasma emission was forward-collected on the axis of the laser using a 1024×1024 pixel iCCD camera (Andor iStar) with the intensifier gate triggered by the Nd:YAG Q-switch. The gate delay of the camera (with respect to the incident laser pulse) and the gate integration width were adjusted in time increments ranging from 2 to $30.0 \mu\text{s}$ and from 0.2 to $3.0 \mu\text{s}$, respectively, with the gate width maintained at 10% of the delay time to allow for adequate collection of light by the iCCD as the plasma emission intensity decayed in time. A 1064-nm mirror was placed in front of the camera to protect the iCCD system from laser radiation transmitted through the plasma, which was measured to be $\sim 10\%$

of original laser pulse energy. In addition, a narrowband interference filter (3-nm full width at half-maximum) centered at 396.2 nm was placed in the optical path. The filter functioned to collect calcium atomic emission, as described above, as well as plasma continuum emission over the same narrow spectral range. An ultraviolet-grade achromatic lens (79.6-mm focal length) was used to focus the plasma image onto the iCCD. Using a finely spaced test grid, the magnification and resolution of the imaging system were found to be $3.6\times$ and $5.3 \mu\text{m}/\text{pixel}$, respectively. The image size and subsequent data transmission rate (i.e., frame capture rate) limited the laser repetition rate to 1 Hz.

For the particle measurements, 1 g of microspheres was diluted with 400 mL of ultrapure DI water to make a stock suspension, which was then nebulized using 5 L/min of dry HEPA-filtered air to deliver 0.14 mL of suspension/min. The drying system was operated with a coflow of 20 L/min dry HEPA-filtered air to promote transport to the LIBS sample chamber and to ensure sufficient dry out. At each gate delay, a series of image frames was collected while running the aerosol system at steady state. Additionally at each delay, the system was run with pure DI water in the nebulizer (i.e., no particles present) in order to collect background plasma images (i.e., controls). For all experiments, the iCCD detector dark current signal was measured by collecting images with an opaque lens cover in place.

Plasma emission was back-collected on-axis with the laser using a pierced mirror and collection lens and then fiber coupled to a 0.275-m spectrometer with a 2400 groove/mm grating. Spectral data were recorded over a 30-nm window centered at 396 nm using an iCCD camera (Princeton Instruments) with the intensifier gate triggered by the laser Q-switch. The laser was run at 5 Hz for spectral analysis. A dilute aerosol stream (~ 1 aerosol particle sampled/5 laser shots) was generated by diluting the stock particle suspension, noted above, 10:1 with ultrapurified DI water and by increasing the dry air coflow to 40 L/min. To calibrate the spectral response of calcium within the laser-induced plasma, the nebulizer system was seeded with an inductively coupled plasma-grade standard solution of calcium (SPEX CertiPrep) diluted to known concentrations: 0.0 (DI water blank), 2.5, 5.0, and $10.0 \mu\text{g}$ of calcium/mL of solution. For calibration, spectral data were recorded over the identical range of intensifier

gate delays and corresponding widths as noted above. Previous work demonstrated that the mean aerosol diameter from such a calibration scheme was generally less than ~ 100 nm for a range of similar conditions,¹⁷ thereby ensuring a high number density, well-dispersed aerosol system.

RESULTS AND DISCUSSION

To first gain an understanding of the laser-induced plasma characteristics in the absence of any aerosol, plasma images were recorded in HEPA-filtered air, with the intensified camera aligned on-axis with the laser pulse. The plasma images were recorded over a range of temporal delays from 2 to 30 μs following the ~ 10 -ns plasma-initiating laser pulse. A series of 20 individual images was ensemble-averaged for each delay time, which together provided a measure of the temporal evolution of the plasma size and emission intensity. As viewed, the plasma image was primarily circular in shape, and grew essentially linearly with time, yielding average diameters ranging from 2.7 to 3.8 mm corresponding to delay times from 2 to 30 μs following plasma initiation. It is noted that beyond ~ 30 μs , the plasma shape was observed to deviate from the circular structure toward a more annular intensity profile. This atypical structure was observed between delay times from about 30 to 50 μs , after which the measured intensity profile once again took on a circular structure. The plasma emission intensity of the images beyond 30 μs was characterized by a marked decrease, making quantitative analysis difficult; hence, analysis was confined to delay times up to 30 μs . The plasma emission intensity, which corresponds to continuum emission (i.e., recombination and Bremsstrahlung radiation) as averaged about the center of each plasma image, was observed to decay exponentially with time, as typical of laser-induced plasmas. This behavior is consistent with the rapid loss of plasma energy via radiative transfer and corresponds to a sharp drop in plasma temperature and free electron density. Based on previous measurements under comparable experimental conditions, free electron densities are expected to peak at $\sim 3 \times 10^{18}$ cm^{-3} near the end of the initiating laser pulse, dropping to 10^{17} cm^{-3} within the first microsecond.¹⁸

After documenting the baseline plasma conditions, the imaging measurements were repeated with the introduction of the aerosolized borosilicate glass particles (2- μm mean diameter, 0.7- μm standard deviation) to the LIBS sample chamber. The aerosol number density was adjusted via the solution concentration to promote single-particle sampling by the laser-induced plasmas. Upon introduction of the aerosol-laden stream, localized, luminous bursts or "hot spots" were observed in the plasma image. These hot spots were spatially random on an image-to-image basis and comprised only a portion of the overall plasma image. Representative images of particle-sampling plasmas are shown in Figure 2 corresponding to four different plasma delays. The images were recorded using a narrowband (3-nm fwhm) interference filter centered at 396.2 nm, which overlaps with the prominent first ionized calcium (Ca II) atomic emission line at 396.85 nm ($0-25\,192$ cm^{-1}). The hot spots are concluded to correspond to localized calcium atomic emission from particle-derived calcium

atoms, which stand in contrast to the continuum plasma emission about this same bandwidth. No such features were recorded in the absence of borosilicate particles. The current finding of discrete atomic emission is consistent with the spatially resolved spectroscopic measurements recently reported for individual magnesium-rich aerosols.¹⁵

The expansion of these spectral regions with time is characteristic of the rate of atomic diffusion of calcium atoms following dissociation from the solid particles. To quantify the growth of these regions, the diameters of 30 individual atomic emission bursts were averaged for each time delay, over the range of delays from 2 to 30 μs following plasma initiation. A plot of the measured emission burst diameters as a function of delay time is presented in Figure 3, which provides a direct measure of the atomic diffusion time scale. Atomic diffusion coefficients were calculated from the slope of a burst area versus time plot, yielding a value of 0.063 m^2/s at 2 μs and 0.017 m^2/s at 30 μs , with an average diffusion rate of 0.04 m^2/s over the temporal range of 2–30 μs . This value suggests a diffusion time scale, whereby individual particles are dissociated with time and subsequently act as expanding (via atomic diffusion) localized atomic sources in which the corresponding atomic emission is readily distinguished from the background plasma emission. Hieftje et al. reported such a conceptual approach for droplet desolvation and solute–particle vaporization processes in analytical flames and plasmas.¹⁹ The current diffusion rate is consistent with the rates used by Hieftje et al. if one scales by $T^{3/2}$, by assuming a plasma temperature on the order of 15 000 K based on previous measurements.

Figure 4 shows an additional single-particle image recorded with a delay of 2 μs following plasma initiation, within which the location and approximate size of the laser focal spot are indicated. Clearly the particle-derived calcium emission burst is spatially separated from the focal spot of the laser beam; hence, it is concluded that the particle did not directly interact with the laser pulse. It is therefore important to note that, based on the current imaging study, plasma–particle interactions within the laser-induced plasma drive the particle dissociation processes, which are subsequently characterized by spatial nonhomogeneity and microsecond time scales. This is consistent with the previously reported discussion of the role of plasma–particle interactions based on a statistical treatment of particle sampling rates.²⁰

To analyze the rate at which the borosilicate glass particles were dissociated within the laser-induced plasma, one first needs a relationship between the analyte atomic emission peaks and the effective analyte concentration. The Ca II line at 396.85 nm was selected as the analyte peak of interest for quantitative spectral analysis using the atomic emission peak-to-base (P/B) ratio. A series of spectra were recorded and ensemble-averaged such that several hundred individual particle events were sampled for each delay time. The corresponding P/B ratio was calculated using the integrated full peak area of the 396.85-nm calcium emission line divided by the integrated signal of a scaled background spectrum (i.e., no particles present) over the same spectral width. Representative spectra corresponding to single laser-induced plasma events that sampled a borosilicate particle are shown in Figure 5. Clearly observed in the figure is the calcium II emission line at

(17) Hahn, D. W.; Carranza, J. E.; Arsenault, G. R.; Johnsen, H. A.; Hencken, K. *R. Rev. Sci. Instrum.* **2001**, *72*, 3706.

(18) Hohreiter, V.; Carranza, J. E.; Hahn, D. W. *Spectrochim. Acta, Part B* **2004**, *59*, 327.

(19) Hieftje, G. M.; Miller, R. M.; Pak, Y.; Wittig, E. P. *Anal. Chem.* **1987**, *59*, 2861.

(20) Hohreiter, V.; Ball, A.; Hahn, D. W. *J. Anal. At. Spectrosc.* **2004**, *19*, 1289.

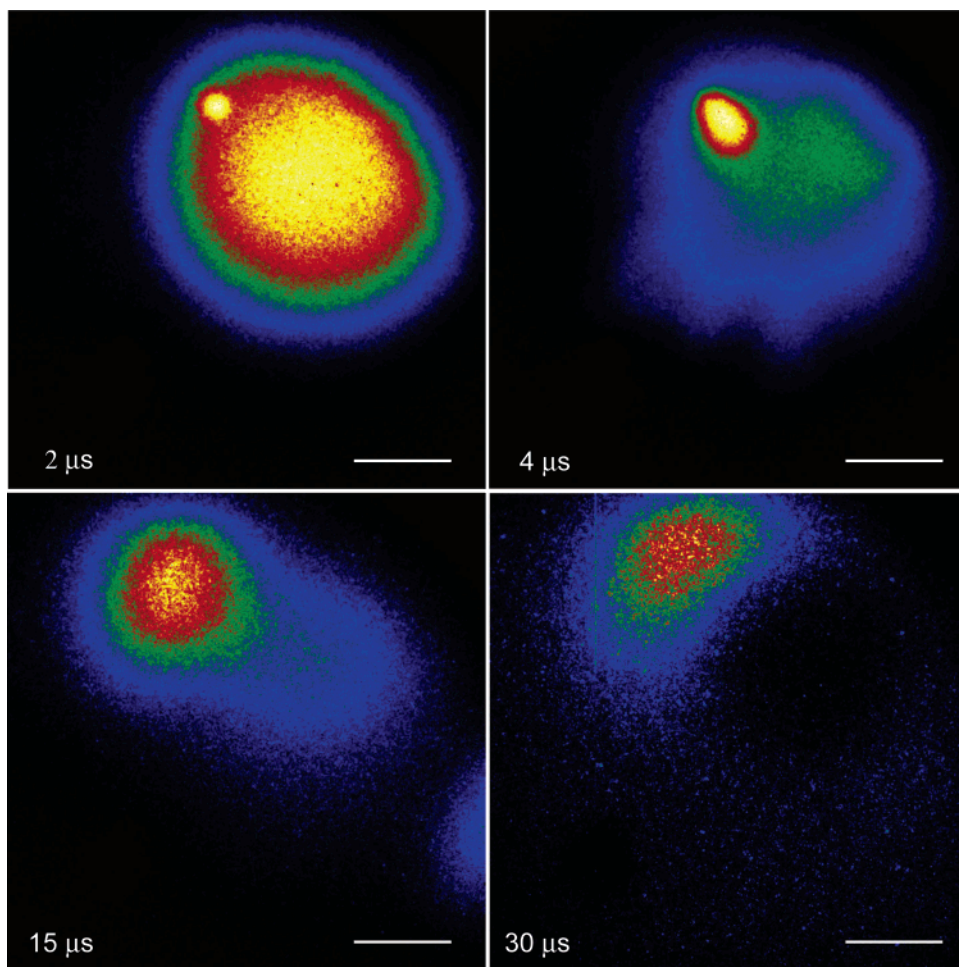


Figure 2. Laser-induced plasma images recorded in the presence of borosilicate glass particles corresponding to delay times of 2, 4, 15, and 30 μs with respect to plasma initiation. Images were recorded using a 396.2-nm narrowband (3-nm fwhm) interference filter. Scale bar, 780 μm .

396.85 nm, as well as the 393.37-nm ($0\text{--}25\,414\text{ cm}^{-1}$) calcium II line. It is noted that these calcium emission lines, with relatively low upper energy states, tend to peak relative to the continuum emission at longer delays; hence, the signal-to-noise ratio (i.e., atomic to continuum emission) is improved in the 30- μs delay spectrum as compared to the 2- μs spectrum. Also present are emission features at 391.4 and 388.4 nm, which are attributed to the N_2^+ first negative system and the CN violet system (primarily at 388.3 and 387.1 nm), noting that the $\sim 388\text{-nm}$ line is a combination of these two molecular lines. The resulting P/B values for the borosilicate aerosol streams were then measured and compared with the appropriate calibration curves at each intensifier delay time (from 2 to 30 μs). This spectral analysis provided a quantitative measure of the equivalent calcium concentration (analyte mass per volume) per borosilicate particle as a function of time following plasma initiation.

To then calculate an absolute mass of calcium derived from the aerosol particles at each delay time, a clear relationship between the spectrally derived equivalent calcium concentration and the measured full plasma volume (as based on the recorded images reported above) is required. Following the analysis of Hahn and Lunden,⁷ the absolute analyte mass is readily determined by the product of the equivalent analyte concentration (via spectral analysis) and the measured effective plasma volume (via

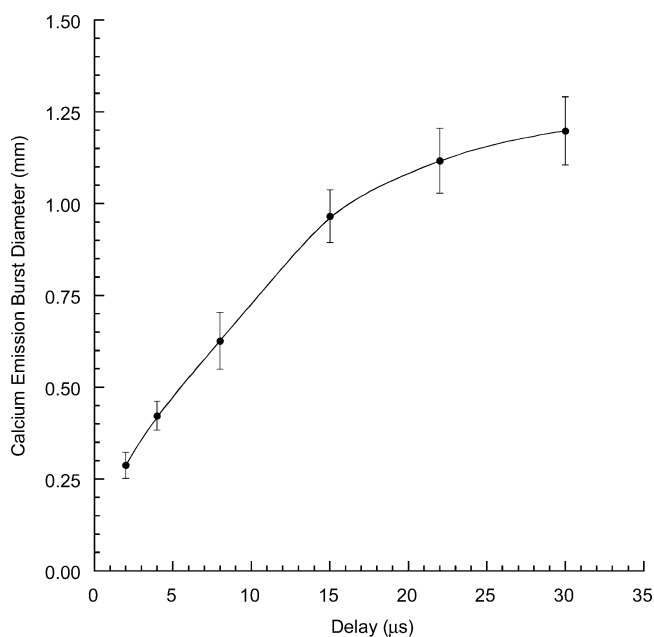


Figure 3. Mean diameter of calcium atomic emission bursts resulting from individual borosilicate glass particles as a function of delay time with respect to plasma initiation. Error bars represent ± 1 standard deviation ($N = 30$).

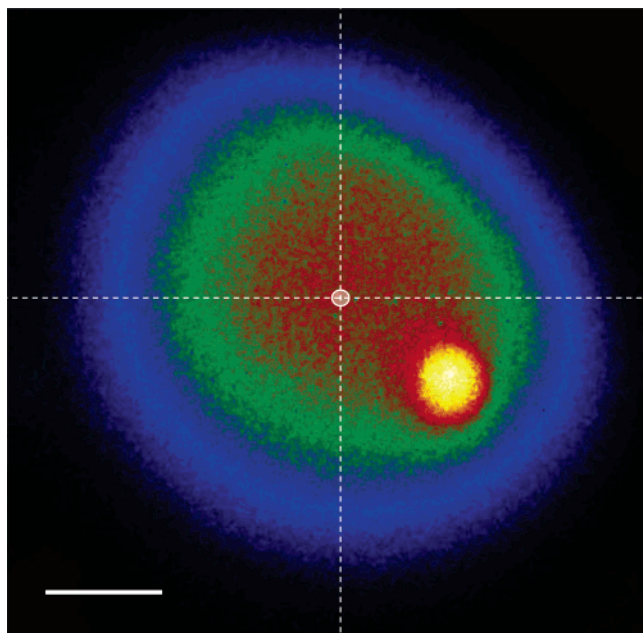


Figure 4. Laser-induced plasma image recorded in the presence of a borosilicate glass particle corresponding to a delay times of $2 \mu\text{s}$ with respect to plasma initiation. Image was recorded using a 396.2-nm narrowband (3-nm fwhm) interference filter. The approximate position and size of the plasma-initiating laser pulse are shown by the crosshairs. Scale bar, $600 \mu\text{m}$.

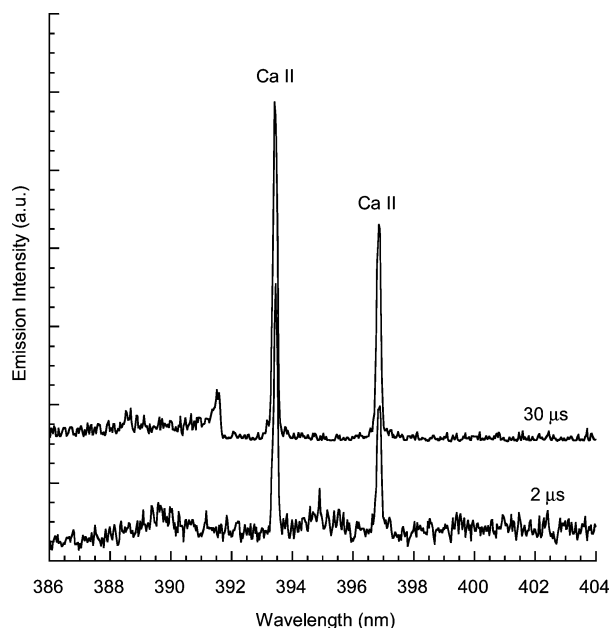


Figure 5. Representative single-shot spectra taken at 2- and $30\text{-}\mu\text{s}$ delay depicting the evolution of the continuum plasma emission and the calcium II lines at 393.37 and 396.85 nm . The spectra have been shifted vertically for clarity and do not reflect the same intensity scale.

image analysis). Together, the plasma image data and the spectral data provide a temporally resolved measure of the dissociated calcium mass, as presented in Figure 6. The asymptotic limit of the Figure 6 data indicates that $\sim 400 \text{ fg}$ of calcium is released within the laser-induced plasma volume from an average borosilicate particle. The 400 fg of calcium corresponds to 2% calcium (by mass) within an average borosilicate particle, based on the reported mean particle diameter of $2 \mu\text{m}$, $0.7\text{-}\mu\text{m}$ standard

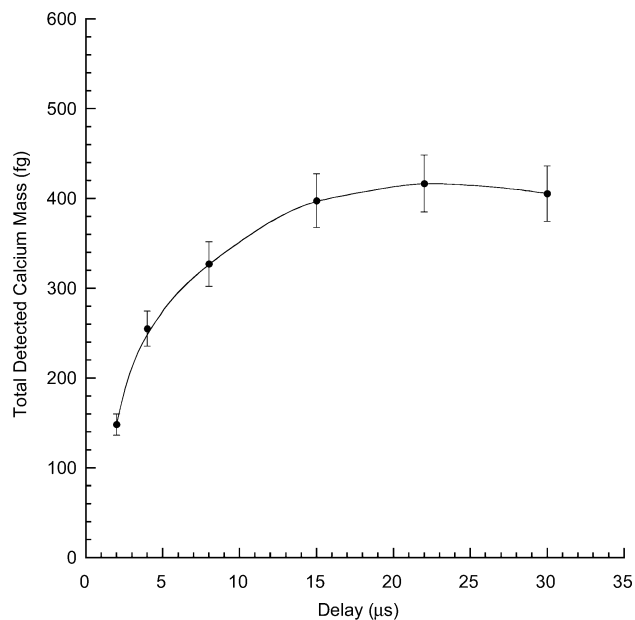


Figure 6. Average LIBS-based mass of elemental calcium detected per laser-induced plasma corresponding to the aerosolized borosilicate glass microspheres as a function of time following plasma initiation.

deviation, particle density of 2.5 g/cm^3 , and an assumed log-normal particle size distribution function. No independent measurement of calcium concentration in the particles was performed, but the 2% value is consistent with a range of borosilicate glasses as reported within the industry.

The plateau in Figure 6 suggests that the number of emitting calcium atoms has approached a limiting value; hence, the plasma has fully dissociated the calcium-containing particle by $\sim 15 \mu\text{s}$ from the end of the laser pulse, with only partial dissociation occurring before this time. Therefore, the concept of a finite rate (and possibly a rate limit) with regard to particle dissociation within a laser-induced plasma, as first put forth by Carranza and Hahn,¹⁶ is strongly supported. In that work, the authors observed that while many orders of magnitude more energy exists in the focused laser pulse than exists in the bond energy of a given solid particulate, the measurable spectral signal, which is directly proportional to atomically dissociated analyte mass in the plasma volume, experienced a plateau as particle size reached a critical value just beyond $2 \mu\text{m}$. It is proposed here that dissociation processes may plateau at some critical value of plasma energy, electron density, or both, hence a corresponding time scale. This suggests that once the plasma has lost significant energy via radiative transfer, it may no longer be energetic enough to dissociate additional mass (i.e., to atoms) of larger particles at the appreciable rate necessary for complete dissociation at the time scale of tens of microseconds. This observation suggests an interesting theoretical model whereby both thermal transport (via convective/conductive processes) and free-electron interaction effects are considered in concert with regard to particle dissociation within a laser-induced plasma. The roles of heat and mass transfer have been reported for relatively cooler analytical flames and thermal plasmas,^{19,21,22} although the current laser-induced

(21) Chen, X.; Pfender, E. *Plasma Chem. Plasma Proc.* **1982**, *2*, 185.

(22) Horner, J. A.; Hieftje, G. M. *Spectrochim. Acta, Part B* **1998**, *53*, 1235.

plasma is characterized by orders of magnitude enhancement in free electron density and significantly higher temperatures, hence the additional interest in direct electron–particle interactions.

If one considers a rate-limiting process for particle dissociation, then if the entrained particle is sufficiently small to be fully dissociated within the period of high reactivity, a linear analyte emission response will be realized. If, however, a particle is too large, complete dissociation will not occur within sufficient time (approximately tens of microseconds), indicating a limit to the mass or particle size that can be fully dissociated and ionized by a single plasma event. The atomic emission response will then level off at a much lessened rate of release, resulting in an effective saturation (i.e., plateau) with respect to atomic dissociation and analyte emission response from the bulk aerosol particle.

The current study suggests a temporal analogue to previous work,¹⁶ leading to the conclusion that aerosol particles entrained in the plasma volume are dissociated (either fully or partially, depending on size) during the time that the plasma volume is sufficiently energetic (within $\sim 15 \mu\text{s}$ in the current study), and subsequently experiences an asymptotic flattening in the analyte atomic emission response thereafter. Such a breakpoint is indicative that the rapid plasma-induced dissociation processes (e.g., electron impact) have given way to much slower processes (e.g., thermal transport via conduction/convection). Irrespective of the exact plasma–particle processes, which may be quite complex, the present study demonstrates that it is the expanded plasma that interacts with the particle, not the laser pulse itself, as noted above.

While the current polydisperse size distribution of borosilicate particles prevents a careful statistical analysis of the shot-to-shot variation of single-particle hits due to the uncertainty of the exact analyte mass on a given shot, several observations are noted. First, the calcium atomic emission P/B ratio was calculated for individual images by averaging the intensity of the localized calcium atomic emission burst and normalizing by the adjacent continuum emission intensity. The temporal behavior of the image-based P/B ratios was very comparable to that of the spectroscopic-based P/B ratios (as described above), noting that the former correspond to a spatially resolved measurement, while the latter data correspond to a spatially averaged measurement. Notwith-

standing the differences in methodology, these two processes should be in temporal agreement, although the spatially resolved (i.e., image-based) measurements might afford an opportunity for enhanced signal-to-noise ratios, as suggested recently by Lithgow and Buckley.¹⁵ Second, for a given delay time, the P/B ratio of individual particle hits was correlated against the radial position of the emission burst with respect to the overall plasma center. For the limited number of hits examined at each delay ($N = 30$), no clear correlation between signal and position was observed for the various delay times; hence, it is difficult to predict what improvements, if any, in analytical figures of merit might arise from such spatially resolved measurements.

In summary, the current results provide direct evidence that atomic emission ensuing from aerosol-derived species is spatially localized over a time scale of tens of microseconds. Furthermore, while optically measurable diffusion of atomic species from aerosol particles occurs within the laser-induced plasma during the time period of spectral emission, these atomic species fail to occupy the entire plasma volume over the range of delay times typically used in LIBS measurements. However, this is not to say that the LIBS technique is limited in the ability to quantify particle-derived analyte concentrations by such spatial nonhomogeneities in plasma emission, as numerous studies have demonstrated just such quantitative measurements. Rather, the current study suggests a discernible time scale for the dissociation of aerosol particles and subsequent atomic diffusion within a laser-induced plasma. To further advance the analytical rigor of laser-induced plasma spectroscopy, rate-limited particle dissociation and atomic diffusion should be further explored in the context of LIBS, as well as for plasmas from other sources and plasma interactions with other forms of matter.

ACKNOWLEDGMENT

This work was supported in part by the National Science Foundation through Grant CTS-0317410.

Received for review October 19, 2005. Accepted December 9, 2005.

AC051872S